

# Photopyroelectric spatially resolved imaging of thermal wave fields

Marek Mieszkowski and Andreas Mandelis

Photoacoustic and Photothermal Sciences Laboratory, Ontario Laser and Lightwave Research Center,  
Department of Mechanical Engineering, University of Toronto, Toronto M5S 1A4, Canada

Received July 22, 1989; accepted November 22, 1989

Spatially resolved photothermal scanning imaging of metallic samples using the photopyroelectric (P<sup>2</sup>E) effect is reported. Unlike that for conventional photothermal detection, the new instrumentation involves polyvinylidene fluoride (PVDF) thin pyroelectric film and a metal-tip detection geometry, which permits monitoring of the local values of the laser-induced diffractive and/or interferometric thermal-wave field in a sample. The effects of the relative PVDF surface-tip position, of the laser beam modulation frequency, and of the presence of subsurface defects in the sample on the spatial resolution of the P<sup>2</sup>E images are examined.

## INTRODUCTION

The emergence of thin-film photopyroelectric (P<sup>2</sup>E) detection as a convenient photothermal method with considerably more degrees of freedom than photoacoustic imaging (both microphonic<sup>1</sup> and piezoelectric<sup>2</sup>) and a back-detection character, as opposed to the photothermal-beam deflection front-detection character,<sup>3</sup> has been well documented.<sup>4</sup> Conventional pyroelectric detection of thermal waves used in a scanned, spatially integrated detection mode has also been reported.<sup>5</sup> A rigorous approach to the calculation of the local P<sup>2</sup>E wave field in the back surface of a sample has been presented recently.<sup>6</sup> The diffraction-integral approach of that formalism treated the back surface as the photothermal wave diffraction screen (or observation plane), and the cross section of the incident exciting laser beam with the front surface as the aperture (or aperture plane). Simultaneously, the development of P<sup>2</sup>E instrumentation capable of sampling the local photothermal-wave- (temperature-) field values in the back of a sample permitted spatially resolved scans of this field.<sup>7</sup> An equivalent experimental method of local thermal-wave-field sampling was nicely illustrated in earlier work by Busse and Renk.<sup>8</sup> The ability of the new instrumentation to measure the local values of the thermal-wave-diffraction field based on the P<sup>2</sup>E principle (as well as the earlier photothermal research<sup>8</sup> based on radiometric principles) has raised the possibility of three-dimensional P<sup>2</sup>E scanning imaging with accurate depth-resolved information on subsurface structures, unlike the projectional, two-dimensional character of other, earlier photothermal-detection schemes.<sup>1-3,5</sup> In this paper we present the salient features of the first spatially resolved diffractive P<sup>2</sup>E scanning imaging and the effects of various instrumental and thermal-wave-field parameters on image quality and resolution from intact samples, as well as samples with subsurface defects.

## IMAGING TECHNIQUE AND EXPERIMENTAL METHOD

Laser photothermal excitation of harmonically modulated intensity generates a spatially well-defined thermal-wave

source in a sample. A new capacitively coupled technique reported earlier<sup>7</sup> is capable of measuring the ac temperature field propagating through a sample in intimate contact with a thin polyvinylidene fluoride (PVDF) pyroelectric film. For spatially resolved measurements the back surface of PVDF must not be electroded, so that the local ac electric field may be sampled. This ac electric field is the result of surface charge density fluctuations due to the P<sup>2</sup>E effect,<sup>9</sup> and they generate an ac voltage across the PVDF surfaces given by<sup>7</sup>

$$U_{ac}(x, y, \omega t) = \frac{p}{\epsilon a^2} \int_{-a/2}^{a/2} \int_{-a/2}^{a/2} \int_0^{L_{PVDF}} T_{ac}(x + x', y + y', z) \times \sin[\omega t + \psi(x + x', y + y', z)] dz dx' dy'. \quad (1)$$

In Eq. (1),  $U_{ac}$  is the ac voltage at modulation frequency  $f = \omega/2\pi$  synchronous to the modulated laser beam, observed between the plates of the effective capacitor at position  $(x, y)$  on the PVDF film.  $p$  is the PVDF pyroelectric coefficient ( $3 \times 10^{-5} \text{C/m}^2 \text{K}$ ),  $\epsilon$  is the film dielectric constant (12 for Kynar PVDF),  $a$  is the dimension of the tip of a detector pin facing the unelectroded surface of PVDF,  $T_{ac}(x, y, z)$  is the amplitude of the ac component of the temperature field in the pyroelectric film, and  $\psi(x, y, z)$  is the phase of the ac component of the temperature field in relation to the phase of modulated light.

A schematic diagram of the detection principle used for P<sup>2</sup>E scanned imaging is shown in Fig. 1. In this particular arrangement the metal- (brass-) tip diameter was 0.8 mm, the focused laser beam waist was 0.1 mm, and the PVDF thickness was 28  $\mu\text{m}$ . Figure 2 shows an outline of the experimental configuration. Details of the system signal-to-noise ratio optimization, as well as equivalent electrical circuitry considerations and modeling, have been reported.<sup>7</sup> An important feature of the imaging geometry of Fig. 1 is its ability to measure P<sup>2</sup>E signals with the probe tip in contact with the PVDF film (purely thermal-wave mode) or remotely, i.e., in a noncontact manner (thermal-wave/capacitive mode) with the measured P<sup>2</sup>E voltage being created across the capacitance formed between the PVDF thin-film upper electrode and the metal-probe pin. This type of signal generation depends on changes in the amount of pyroelectrical-

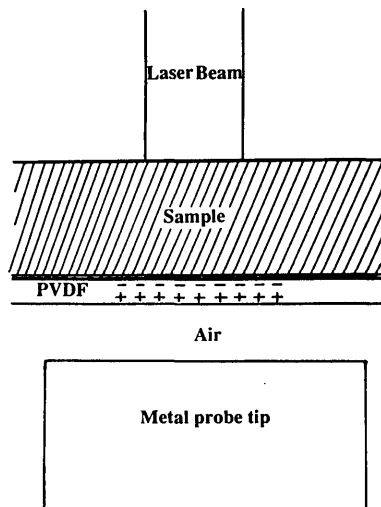


Fig. 1. Schematic diagram of the capacitively coupled pyroelectric geometry used for P<sup>2</sup>E spatially resolved imaging in condensed-phase materials.

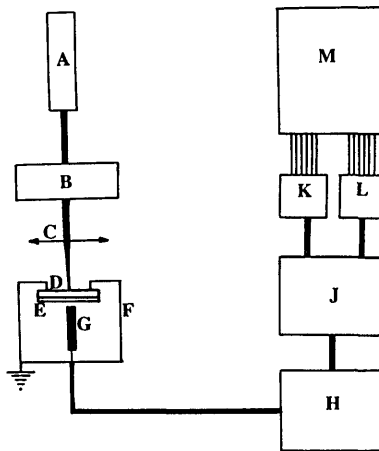


Fig. 2. Schematic diagram of scanning P<sup>2</sup>E imager: A, 10-mW He-Ne laser, Hughes Aircraft Company Model 3235H-PC; B, mechanical chopper, AMKO Model OC-4000; C, focusing lens; D, sample; E, PVDF film; F, metal shield; G, brass tip; H, preamplifier, Ithaco Model 1201; J, lock-in analyzer, EG&G Model 5204; K, in-phase signal to channel 0 of analog-to-digital converter; L, quadrature signal to channel 1 of analog-to-digital converter (Lab Master board from Tecmar); M, microcomputer, IBM PS Model 30.

ly generated charges on the effective capacitor plates owing to the P<sup>2</sup>E effect, followed by concomitant variations in the interplate electric field. P<sup>2</sup>E images obtained in this study were generated by keeping the metallic tip fixed below the PVDF lower surface and scanning the laser beam across the upper surface of the sample. Thus, in principle, our P<sup>2</sup>E images consisted of photothermal-wave-field diffraction patterns, the spatial-resolution limits of which were determined by the spatial extent of the tip<sup>6</sup> [Eq. (1)].

## RESULTS AND DISCUSSION

### Intact Sample Imaging

For reasons of enhanced contrast between the P<sup>2</sup>E temperature field and the inherent instrumental background contributing to baseline noise, all scans reported below are

shown between maximum and half-maximum values of absolute signal amplitude intensity and phase shift. Figure 3 shows amplitude and phase scans of a uniform aluminum sample, 1.5 mm thick, at 50-Hz modulation frequency. The probe pin is in contact with the back surface of the PVDF detector. The signal-amplitude maximum and the phase-shift extremum (actually a minimum shift with respect to the phase of modulated laser light) correspond to the closest distance between the aperture (i.e., the laser beam position) and the probing pin tip. In general the phase signal exhibits higher spatial confinement than the amplitude signal. This ultimately amounts to higher phase resolution, a feature of photothermal-wave imaging noticed earlier with spatial depth-integrated photoacoustic detection.<sup>10</sup>

Figure 4 is a repetition of the scans of Fig. 3; however in this image the P<sup>2</sup>E signal is due to capacitive PVDF-probe-tip coupling at an interplate distance of 0.15 mm. The effect of PVDF-metal-tip separation is the contribution to the P<sup>2</sup>E signal of electric field lines from an effective area on the PVDF surface, which is larger than the metal-tip-area projection on it.<sup>11</sup> As a result the spatial resolution is poorer, and the thermal-wave field appears more broadened than that shown in Fig. 3. No particular improvement in the phase spatial resolution is apparent under these conditions.

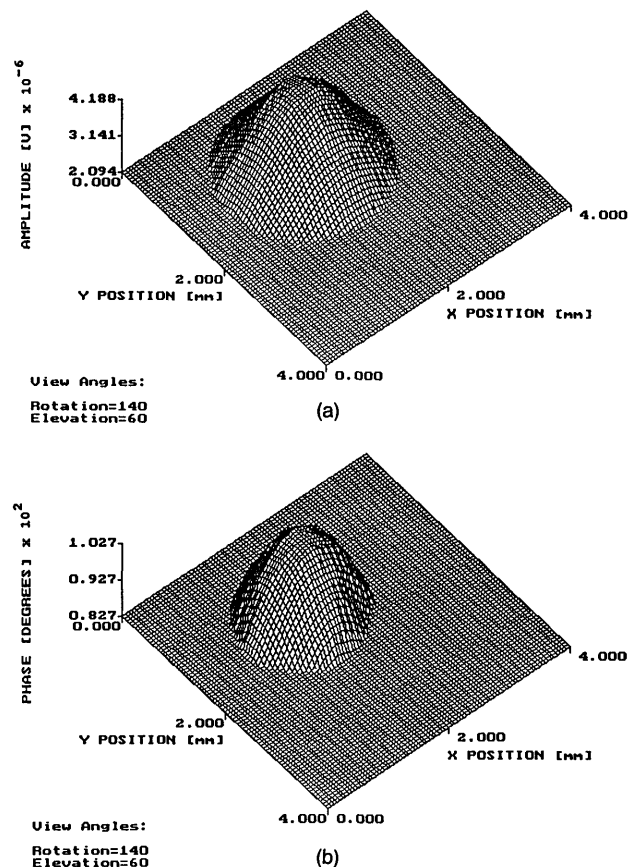


Fig. 3. Amplitude (a) and phase image (b) of the photothermal-wave P<sup>2</sup>E field from an exciting laser beam (0.1 mm in diameter) generated in an aluminum sample (1.5 mm thick) with the probe tip in contact with the backing PVDF detector;  $f = 50$  Hz. In this and later figures view angle definitions are as follows: rotation, angle between Y axis and line of sight (when elevation angle = 0°); elevation, angle between XOY plane and line of sight. Angles are expressed in degrees.

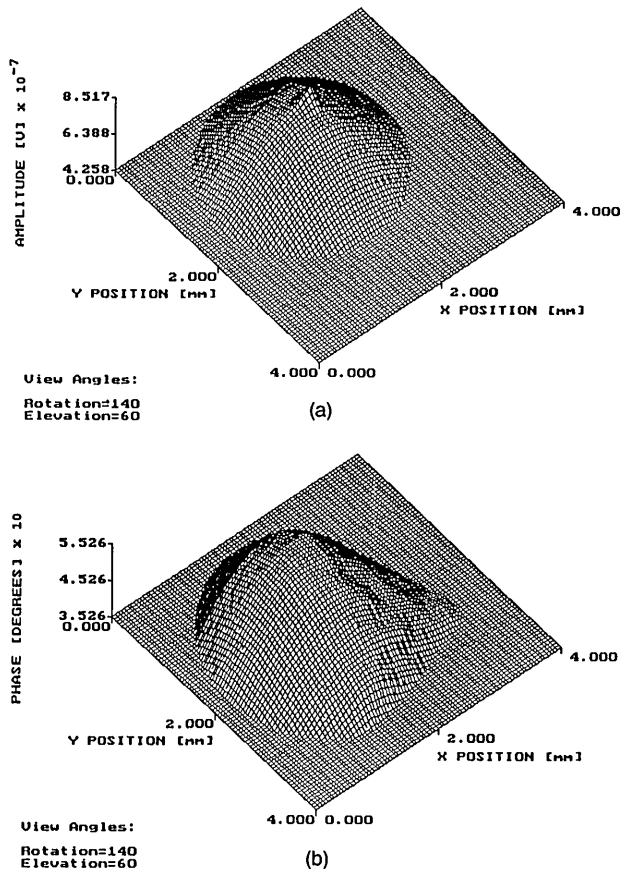


Fig. 4. Amplitude (a) and phase image (b) of the photothermal-wave P<sup>2</sup>E field as in Fig. 3 with a PVDF-metal-tip separation of 0.15 mm;  $f = 50$  Hz.

Figure 5 is indicative of the decrease in spatial resolution with decreased modulation frequency and should be compared with Fig. 3. At the same time the signal is increased by  $\sim 1$  order of magnitude with respect to the  $f = 50$  Hz signal, as expected.<sup>6</sup> The apparent depression exhibited by the amplitude signal, Fig. 5(a), near the position of the maximum is caused by the flaking off of the thin layer of black paint that was applied to the surface of the aluminum sample for absorptivity and signal enhancement. This amounted to an increased reflectivity, accompanied by a decrease in the signal amplitude. It should be noticed that the phase image, Fig. 5(b), shows no evidence of the flaking. This is so because any intensity variations due to the changed surface reflectivity cancel out from the phase channel, which is equal to the ratio of the quadrature and in-phase channels, each of which is proportional to the incident intensity.<sup>12</sup> As a result, the phase scan gives a pure thermal-wave image, free from contributions due to the optical reflectivity of the surface.<sup>10,12,13</sup>

#### Imaging of a Sample with Subsurface Defects

A 1.5-mm-thick aluminum sample, similar to the one described in the preceding subsection, was machined, and a 1.0-mm-diameter hole was drilled out (as shown in Fig. 6). The minimum distance between the hole surface and the irradiated flat surface was 0.2 mm. For these measurements the entire signal range (maximum to minimum) will be re-

ported, so as not to eliminate particular low-level imaging features due to subsurface structure. Figure 6 shows the actual location of the pin tip with respect to the subsurface hole. Figures 7 and 8 are the thermal-wave images resulting from scans at 10 and 30 Hz, respectively. In both figures the signal-amplitude maxima and phase minima are generated with the laser source directly above the position of the pin, as expected. The presence of the hole centered along the  $x = 2$  mm line is more pronounced in the phase images of both scans, as expected from the higher spatial resolution of this channel. A comparison of Figs. 7(b) and 8(b) shows that the phase-image depression along the subsurface feature region is more apparent in the 30-Hz scan, which is therefore of a higher resolution. This trend of an increased depth resolution with increasing modulation frequency has been reported previously<sup>2,14</sup> with respect to thermal-wave imaging with focused infrared photothermal radiometric detection and a fixed laser source-detector distance. In the present experiments, P<sup>2</sup>E images appear asymmetric with respect to the hole position owing to the varying distances between source and probe, a feature not shared with earlier configurations.<sup>14,15</sup> It is important to note that Busse has concluded<sup>15</sup> that spatial resolution in back-surface photothermal-wave transmission phase measurements akin to ours is superior to that exhibited by front-surface photoacoustic phase detection.

In order to suggest that full spatial resolution is responsi-

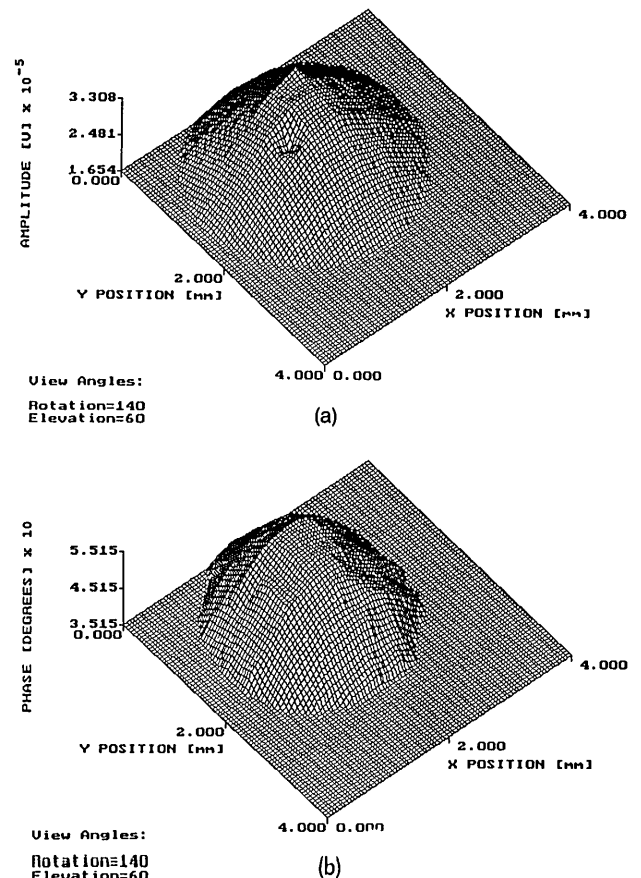


Fig. 5. Amplitude (a) and phase image (b) of the photothermal-wave P<sup>2</sup>E field as in Fig. 3;  $f = 10$  Hz.

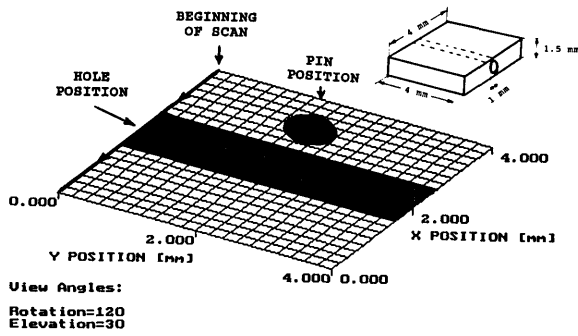


Fig. 6. Geometry of the relative positions between the probe pin and a subsurface hole in an aluminum sample. (The sample is shown in the inset.)

ble for mappings of the thermal-wave interferometric capabilities of our technique, a further set of photothermal-wave images was obtained with the sample oriented as shown in Fig. 9. The pin tip was in full contact for maximum resolution. The effects of increasing modulation frequency on resolution are shown in the maximum-to-half-maximum signal amplitude images of Figs. 10–12. Similar effects are observed in the phase images shown in a range less than 20° below maximum (Figs. 10 and 11) and 60° below maximum (Fig. 12). Two signal lobes are observed in the amplitudes and phases of the Fig. 10 (10 Hz) and Fig. 11 (50 Hz) scans. These peaks are indicative of the existence of boundaries at subsurface structure and should be attributed to back-surface (transmission) thermal-wave enhancement due to thermal-barrier clearing (the air gap) beyond the metal–interstitial air gap (hole) interfaces. Figure 10(b) indicates that the maxima are located at ~0.8 mm away from the central minimum on either side. At  $f = 10$  Hz the thermal-diffusion length in aluminum is<sup>6</sup>

$$\mu_t(10 \text{ Hz}) = (\alpha_{Al}/\pi f)^{1/2} \cong 1.6 \text{ mm}, \quad (2)$$

where  $\alpha_{Al}$  is the thermal diffusivity of aluminum equal to<sup>16</sup> 0.8 cm<sup>2</sup>/sec. For direct thermal-ray transmission to the detector center point P, the minimal translation of the laser beam source from the hole central axis of symmetry (at  $x = 2$  mm) and along the  $x$  direction is [Fig. 10(b) inset]

$$\overline{OA} = \overline{CD} \left[ \frac{\overline{OP}}{\overline{DP}} \right] \approx 1.2 \text{ mm}. \quad (3)$$

The minimal translation for direct transmission to the edge of the pin ( $P'$ ) is given by

$$\overline{OE} = 0.4 \text{ mm} + \overline{FD}' \left[ \frac{\overline{OP}}{\overline{P'D}'} \right] = 0.6 \text{ mm}, \quad (4)$$

where  $\overline{FD}' \approx 0.1$  mm. The average beam position is  $(\overline{OA} + \overline{OE})/2$ , which suggests the dominant thermal-wave transmission contribution to the pin signal for the source position at ~0.9 mm away from the minimum, in agreement with the symmetric lobe maxima positions in Figs. 10–12. The amplitude signal depression on the rightmost peak of Fig. 10(a) is of the same origin as discussed in conjunction with Fig. 5(a) and does not appear in the phase image of Fig. 10(b).

Figure 11 is a repetition of the scans in Fig. 10, obtained at 50 Hz. The improvement of spatial resolution in both channels over the 10-Hz scan is remarkable, especially in the

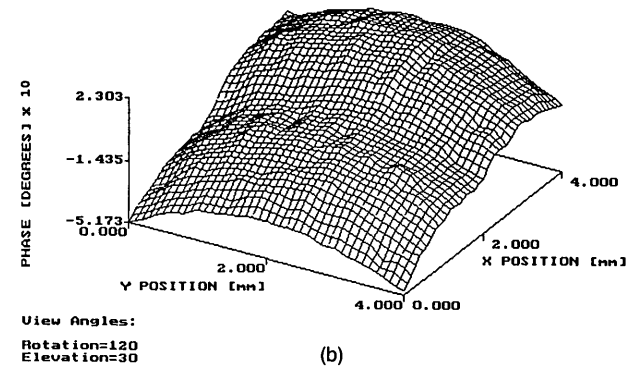
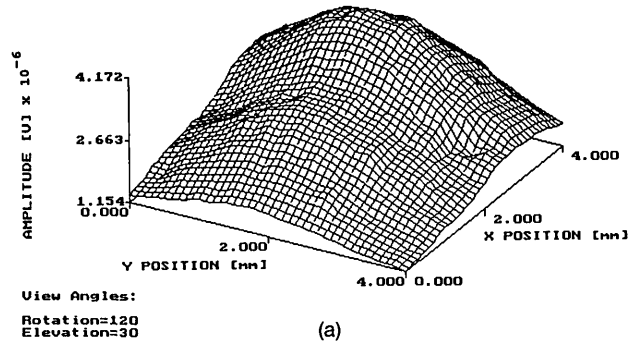


Fig. 7. Amplitude (a) and phase image (b) of P<sup>2</sup>E signal generated in a 1.5-mm-thick aluminum sample with a subsurface hole along the  $x$  axis centered at  $y = 2$  mm and a pin-tip position as in Fig. 6;  $f = 10$  Hz; PVDF-detector-pin separation: 0.15 mm.

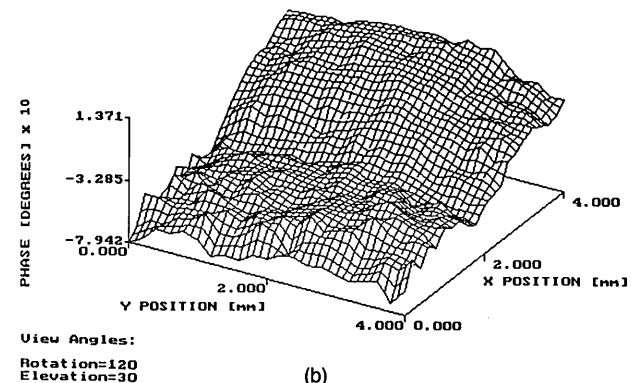
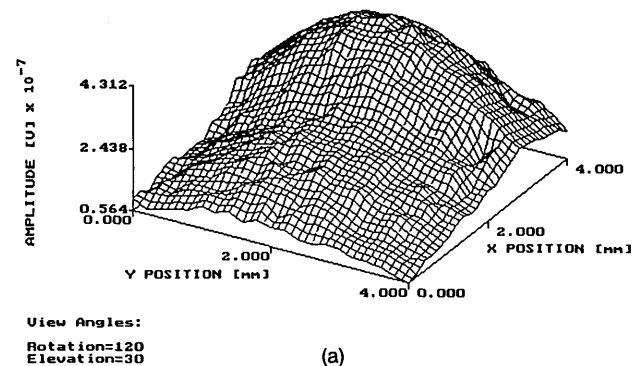


Fig. 8. Amplitude (a) and phase image (b) of P<sup>2</sup>E signal generated as in Fig. 7;  $f = 30$  Hz; PVDF-detector-pin separation: 0.15 mm.

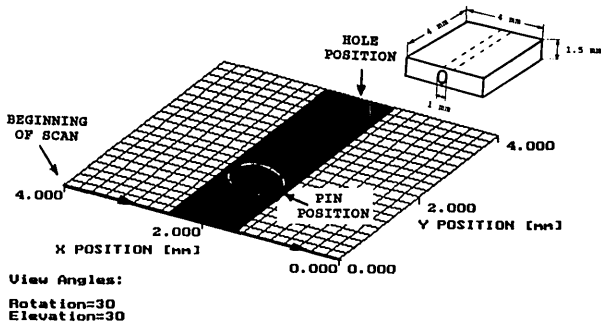
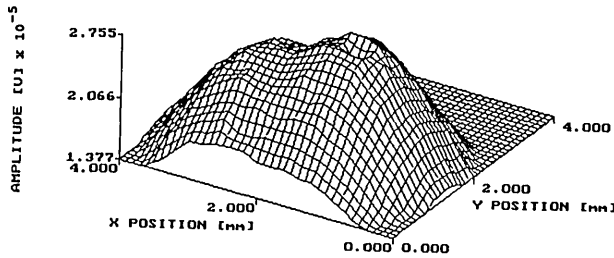
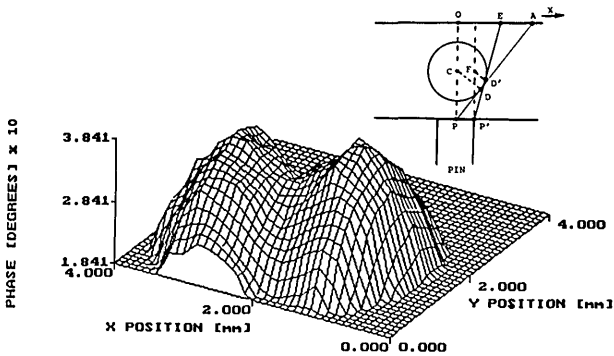


Fig. 9. Another relative configuration between the probe pin and the subsurface hole in the aluminum sample.



View Angles:  
Rotation=30  
Elevation=30

(a)



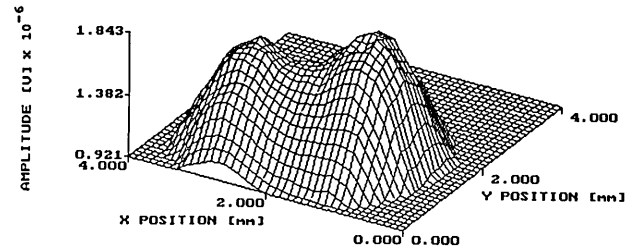
View Angles:  
Rotation=30  
Elevation=30

(b)

Fig. 10. Amplitude (a) and phase image (b) of P<sup>2</sup>E signal generated in the aluminum sample of Fig. 9 with the subsurface hole along the y axis centered at x = 2 mm and a pin-tip position as in Fig. 9; f = 10 Hz; PVDF-detector-pin separation: 0 mm.

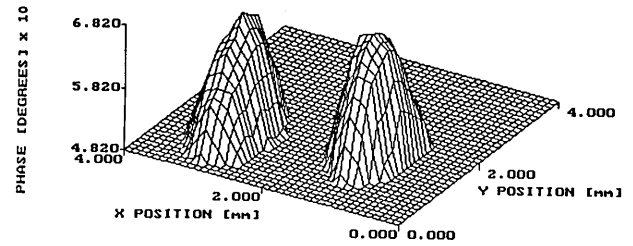
phase channel. The positions of the lobe maxima remain unchanged, in agreement with the simple thermal-ray transmission considerations above. The exponential decay of the thermal-wave-diffraction field propagation in the sample<sup>6</sup> is expected to dampen nondirect line-of-sight contributions to the pin signal much more efficiently at 50 than at 10 Hz: the much enhanced resolution is a result of the spatially damped nature of these pseudowaves. When the modulation frequency is increased to 100 Hz or above, an interesting feature appears in the amplitude images: a central maximum located between the two lobes emerges, and its relative size increases with *f*. Figure 12(a) shows this situation for *f* = 115 Hz. The peak positions of the sidelobes remain unchanged compared with those of Figs. 10 and 11, while the central lobe has its maximum along the *x* = 2 mm axis of the subsurface hole. The phase image, Fig. 12(b), also shows an increased intravalley contribution compared to Fig. 11(b).

Such phase shifts were also found to increase with increasing modulation frequency and are indicative of the thermal-wave origin of the intravalley feature. The thermal-diffusion length at 115 Hz is 0.47 mm in aluminum, and therefore P<sup>2</sup>E imaging would tend to enhance features closer to the front surface of the sample, as previously observed with depth-integrating two-dimensional scans using photoacoustic<sup>17</sup> and photothermal<sup>18</sup> detection. The spatially resolved three-dimensional diffractive nature of the present technique renders it sensitive to photothermal-diffraction phe-



View Angles:  
Rotation=30  
Elevation=30

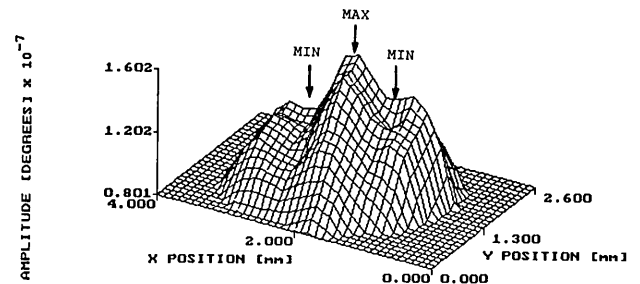
(a)



View Angles:  
Rotation=30  
Elevation=30

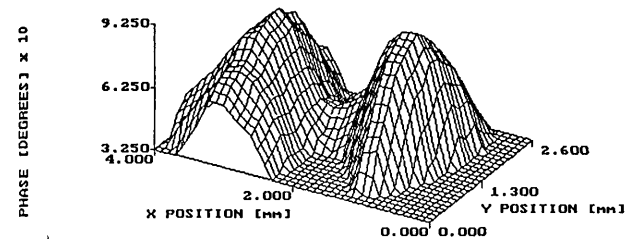
(b)

Fig. 11. Amplitude (a) and phase image (b) of P<sup>2</sup>E signal generated as in Fig. 10; f = 50 Hz; PVDF-detector-pin separation: 0 mm.



View Angles:  
Rotation=30  
Elevation=30

(a)



View Angles:  
Rotation=30  
Elevation=30

(b)

Fig. 12. Amplitude (a) and phase image (b) of P<sup>2</sup>E signal generated as in Fig. 10; f = 115 Hz; PVDF-detector-pin separation: 0 mm.

nomena,<sup>6</sup> which are largely absent from integrating one- or two-dimensional detection schemes, such as the one-dimensional thermal-wave interference effects described by Bennett and Patty.<sup>19</sup> It is therefore believed that the central lobe of Fig. 12 is associated with thermal-wave diffraction and constructive interference within the aluminum mass between the front surface of the sample and the upper surface of the subsurface hole, equivalent to the phenomenon of enhanced optical transmission through interference in a thin transparent plate (fringing). More research will be required to establish the main communication pathway of such interfering thermal waves to the back surface and the detection pin. Two possibilities are evident: the path lies either directly through the intervening gas (air) or sideways through the aluminum mass adjacent to the hole boundaries. The latter pathway seems more plausible as the thermal wavelength at 115 Hz in aluminum is<sup>6</sup>

$$\lambda_t(115 \text{ Hz}) = 2\pi(\alpha_{Al}/\omega)^{1/2} \approx 2.1 \text{ mm}, \quad (5)$$

long enough for circumferential communication with the pin position. Furthermore, the large thermal mismatch at the aluminum-air interface would tend to reflect upward away from the back-surface detector, most of the energy imparted into the thermal wave.<sup>9</sup> This effect would result in an enhanced photothermal signal if a front-surface detection technique were used, a well-known fact of photoacoustic microscopy.<sup>5</sup>

## CONCLUSIONS

The salient features of a new P<sup>2</sup>E spatially resolved diffractive thermal-wave imaging technique have been presented. Enhancement of spatial resolution with increased modulation frequency and decreased PVDF surface-detector pin distance has been demonstrated. The interferometric nature of the present method has been suggested through constructive interference phenomena observed at elevated modulation frequencies resulting in thermal diffusion lengths comparable to material subsurface structures. This unique feature is expected to lead to the development of photothermal wave tomography.<sup>20</sup>

## ACKNOWLEDGMENT

The support of the Ontario Laser and Lightwave Research Center and of the National Science and Engineering Research Council of Canada is gratefully acknowledged.

## REFERENCES

1. H. Y. Wong, R. L. Thomas, and G. F. Hawkins, "Surface and subsurface structure of solids by laser photoacoustic spectroscopy," *Appl. Phys. Lett.* **32**, 538-539 (1978).

2. A. Rosencwaig, "Photoacoustic microscopy," *Am. Lab.* **11**, 39-49 (1979).
3. L. D. Favro, P.-K. Kuo, and R. L. Thomas, "Thermal wave propagation and scattering in semiconductors," in *Photoacoustic and Thermal Wave Phenomena in Semiconductors*, A. Mandelis, ed. (North-Holland, New York, 1987), Chap. 4, p. 75.
4. H. Coufal and A. Mandelis, "Photopyroelectric spectroscopy of semiconductors," in *Photoacoustic and Thermal Wave Phenomena in Semiconductors*, A. Mandelis, ed. (North-Holland, New York, 1987), Chap. 7, p. 149.
5. M. Luukkala, "Photoacoustic microscopy at low modulation frequencies," in *Scanned Image Microscopy*, E. A. Ash, ed. (Academic, London, 1980), p. 273; C. R. Petts and H. K. Wikramasinghe, "Photothermal spectroscopy on a microscopy scale," in *Proceedings of the Institute of Electrical and Electronics Engineers Ultrasonic Symposium* (Institute of Electrical and Electronics Engineers, New York, 1981), pp. 832-836.
6. A. Mandelis, "Theory of photothermal-wave diffraction and interference in condensed media," *J. Opt. Soc. Am. A* **6**, 298-308 (1989).
7. M. Mieszkowski, K. F. Leung, and A. Mandelis, "Photopyroelectric thermal wave detection via contactless capacitive polyvinylidene fluoride (PVDF)-metal probe-tip coupling," *Rev. Sci. Instrum.* **60**, 306-316 (1989).
8. G. Busse and K. F. Renk, "Stereoscopic depth analysis by thermal wave transmission for nondestructive evaluation," *Appl. Phys. Lett.* **42**, 366-368 (1983); G. Busse, "Thermal wave nondestructive depth profiling with stereoscopic photothermal detection," *J. Phys. (Paris) C* **6**, 471-474 (1983).
9. A. Mandelis and M. M. Zver, "Theory of photopyroelectric spectroscopy of solids," *J. Appl. Phys.* **57**, 4421-4430 (1985).
10. G. Busse and A. Rosencwaig, "Subsurface imaging with photoacoustics," *Appl. Phys. Lett.* **36**, 815-818 (1980).
11. A. Mandelis, "A variational-Green's function approach to theoretical treatment and applications of the capacitance of three-dimensional geometries," *Can. J. Phys.* **60**, 179-195 (1982).
12. R. L. Thomas, L. D. Favro, K. R. Grice, L. J. Inglehart, P. K. Kuo, J. Lhota, and G. Busse, "Thermal wave imaging for nondestructive evaluation," in *Proceedings of the Institute of Electrical and Electronics Engineers Ultrasonic Symposium* (Institute of Electrical and Electronics Engineers, New York, 1982), pp. 586-591.
13. A. Mandelis, A. Williams, and E. K. M. Siu, "Photothermal wave imaging of MOS field effect transistor (MOSFET) structure," *J. Appl. Phys.* **63**, 92-98 (1988).
14. G. Busse, "Photothermal transmission probing of a metal," *Infrared Phys.* **20**, 419-427 (1980).
15. G. Busse, "Optoacoustic and photothermal material inspection techniques," *Appl. Opt.* **21**, 107-117 (1982).
16. Y. S. Touloukian, R. W. Powell, C. Y. Ho, and M. C. Nicolaou, *Thermal Diffusivity* (IFI/Plenum, New York, 1973), pp. 2-5.
17. G. Busse and A. Ograbek, "Optoacoustic images," *J. Appl. Phys.* **51**, 3576-3581 (1980).
18. P. E. Nordal and S. O. Kanstad, "Photothermal radiometry for spatial mapping of spectral and material properties," in *Scanned Image Microscopy*, E. A. Ash, ed. (Academic, London, 1980), p. 331.
19. C. A. Bennett and R. R. Patty, "Thermal wave interferometry: a potential application of the photoacoustic effect," *Appl. Opt.* **21**, 49-54 (1982).
20. A. Mandelis and M. Mieszkowski, "Thermal wave sub-surface defect imaging and tomography apparatus," U.S. Patent applied for.